Coronagraphic postprocessing using gradient-based optimization under wavefront drift

Natalia Sanchez-Soria, James R. Fienup
University of Rochester

University of Rochester Hajim School of Engineering & Applied Sciences

The Institute of OPTICS

Introduction

Postprocessing techniques are used to reduce residual starlight in coronagraph images. Conventional postprocessing methods estimate the PSF by using reference images of similar stars, by rotating the telescope, or by probing deformable mirrors. Forward-modeling postprocessing approaches leverage wavefront information to obtain a PSF estimate, without requiring moving the telescope or taking additional images. A gradient-based optimization approach (GBO) was implemented by Feng et al. [1] for the JWST coronagraph, yielding good results. We are interested in how this kind of approach would perform for an Habitable Worlds Observatory (HWO) scenario.

In this work, we implemented a GBO approach using a nonlinear optimizer, L-BFGS, to solve for the wavefront error that results in a simulated image that best subtracts the residual starlight in the target image.

System parameters and assumptions

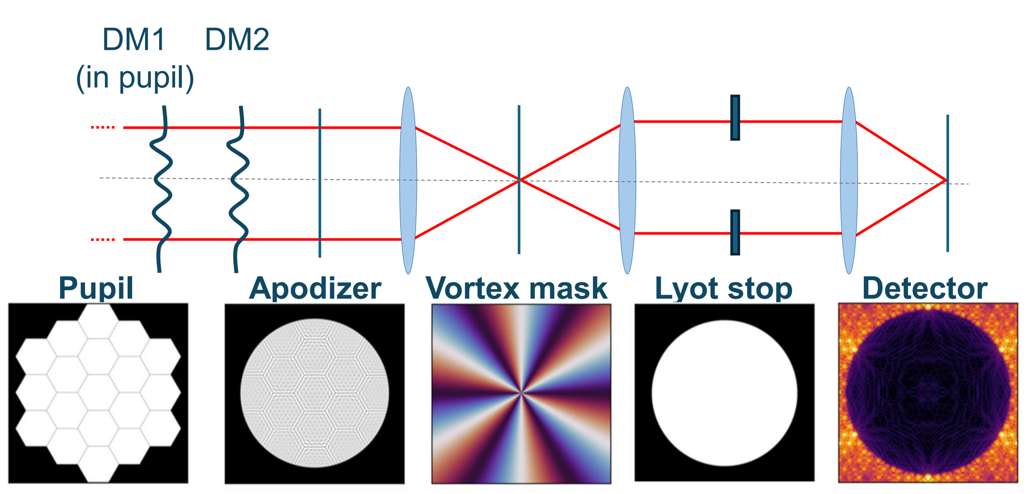

Figure 1. Schematic representation of the AAVC coronagraph design for EAC-1 including two DMs

- Amplitude-apodized vortex coronagraph [2] design for EAC-1 [3]
- Two identical DMs: 96x96 actuators and 1 mm pitch
- Flat spectrum with λ_0 = 550 nm and 10% bandwidth
- Telescope diameter: 6 m (assumed for photometry)
- Target star: Kappa Ceti (m = 4.84, T = 5708K)
- Only Poisson noise

Planet	Radial position $[\lambda_0/D]$	Contrast
Venus	4.509	4.75×10^{-10}
Earth	6.356	9.91×10^{-11}
Jupiter	24.343	3.12×10^{-9}

Wavefront error

We included phase-only aberrations in the pupil plane. We included global Zernike aberrations (Z4-Z15), as well as segment misalignments consisting of a random piston, tip and tilt for each segment.

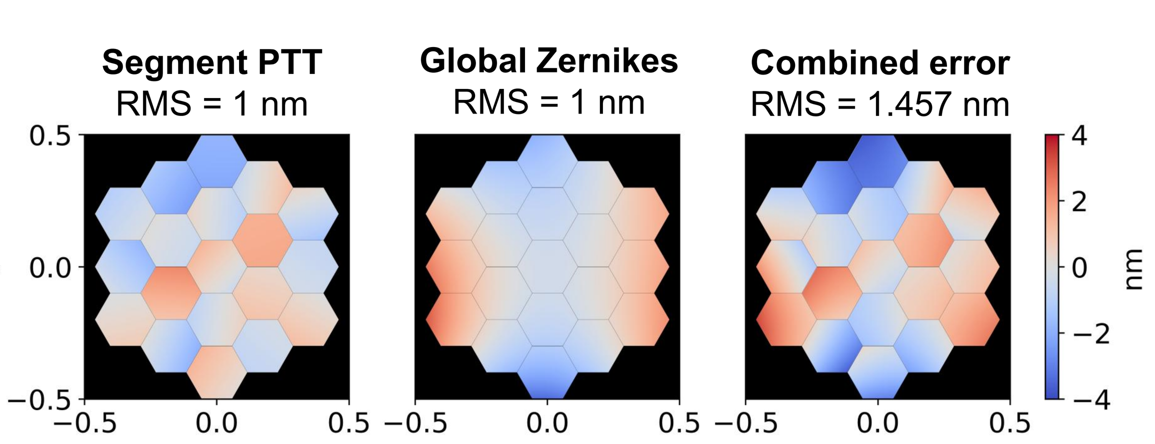

Figure 2. Wavefront error (a) from segment misalignments, (b) from Zernike aberrations, and (c) combined wavefront error. The pupil coordinates (x, y) are normalized with respect to the flat-to-flat telescope diameter.

The initial case was corrected with EFC [4] using two DMs. Then, we simulated the aberrations drifting over time by modelling it as a Gaussian random process. We made either the global Zernikes or the segment alignment drift while keeping the other static.

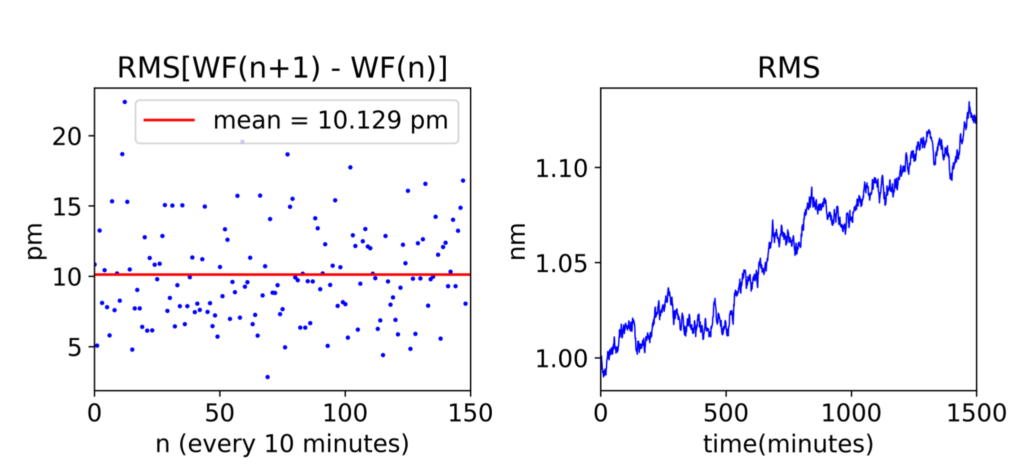

Figure 3. RMS of wavefront difference between 10-minute intervals (a), and total wavefront RMS over time (b) varying as a Gaussian random process, for a case with drift in the Zernike aberrations at a rate of 10 pm RMS per 10 minutes.

Method

Our goal is to solve for a wavefront error (WFE) estimate $\widehat{W}$ that will result in a simulated image that will best subtract the measured stellar speckle pattern; therefore, minimizing an error metric.

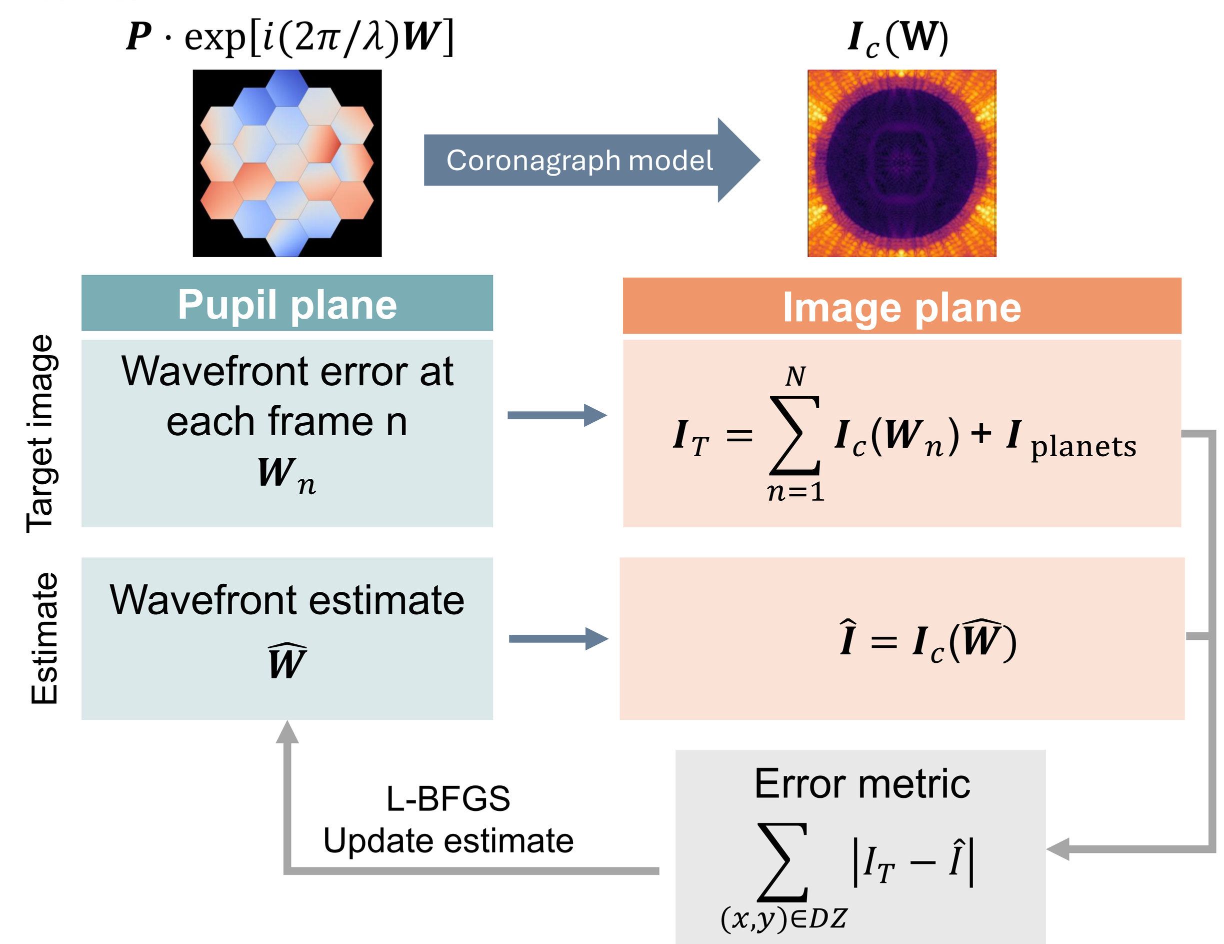

Figure 4. Method schematic.

The starting guess for the wavefront was the WFE at time zero, which was 22.75 hours before starting the observation of the target star. This was chosen in order to simulate a case in which the WFE was not know exactly, and it differed more from the actual wavefront for cases with more drift.

We explored solving for the aberration coefficients (Zernike and segment misalignments) that make up the wavefront, as well as solving on a point-by point basis, using each pixel as a variable. We also tested a combination of both approaches.

Results

Figure 4 shows the normalized error metric at each iteration, as well as the SNR at each planet location, for each optimization approach. Figure 5 shows the resulting image for each approach. Optimizing on a point-by-point basis achieves the lowest final error but it is prone to subtracting planet light thus resulting in the lowest SNR.

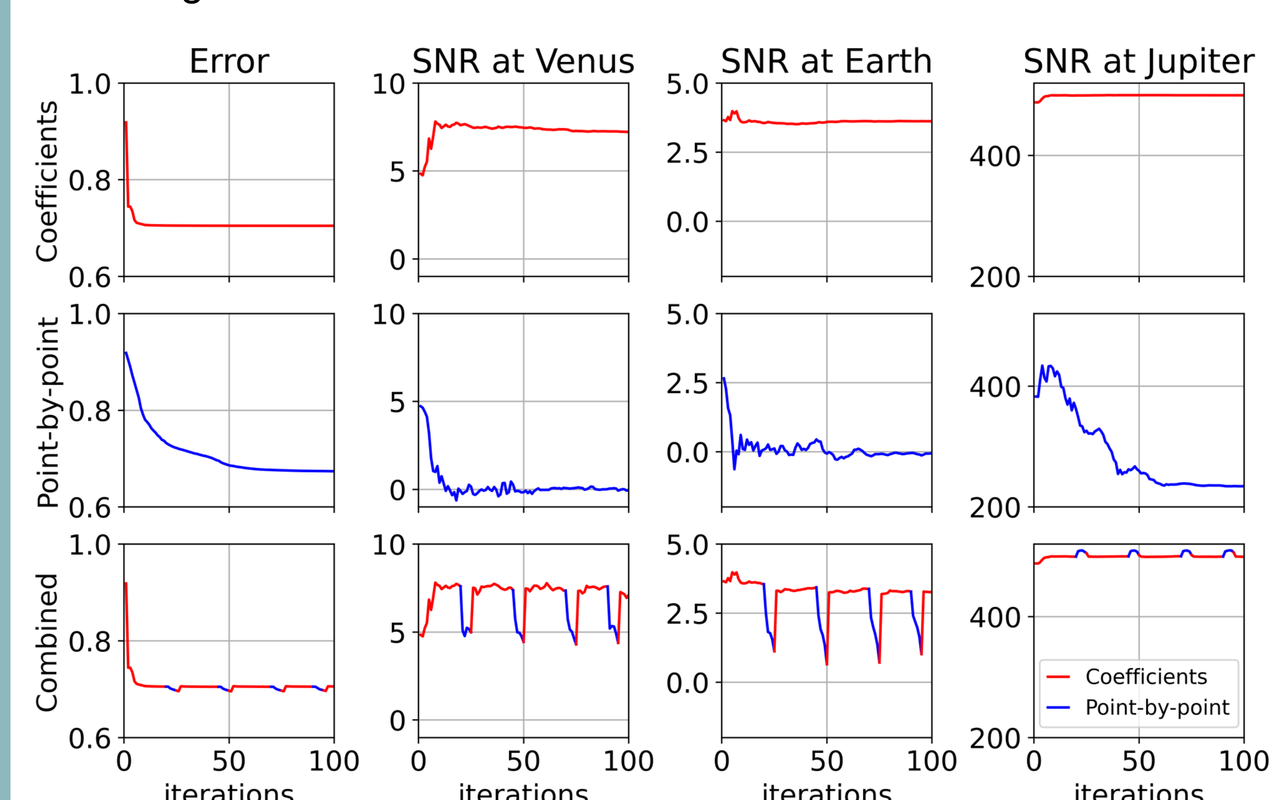

Figure 4. Normalized error and SNR at each planet per iteration. Using different optimization approaches. For a case with Zernike drift of 5pm/10min.

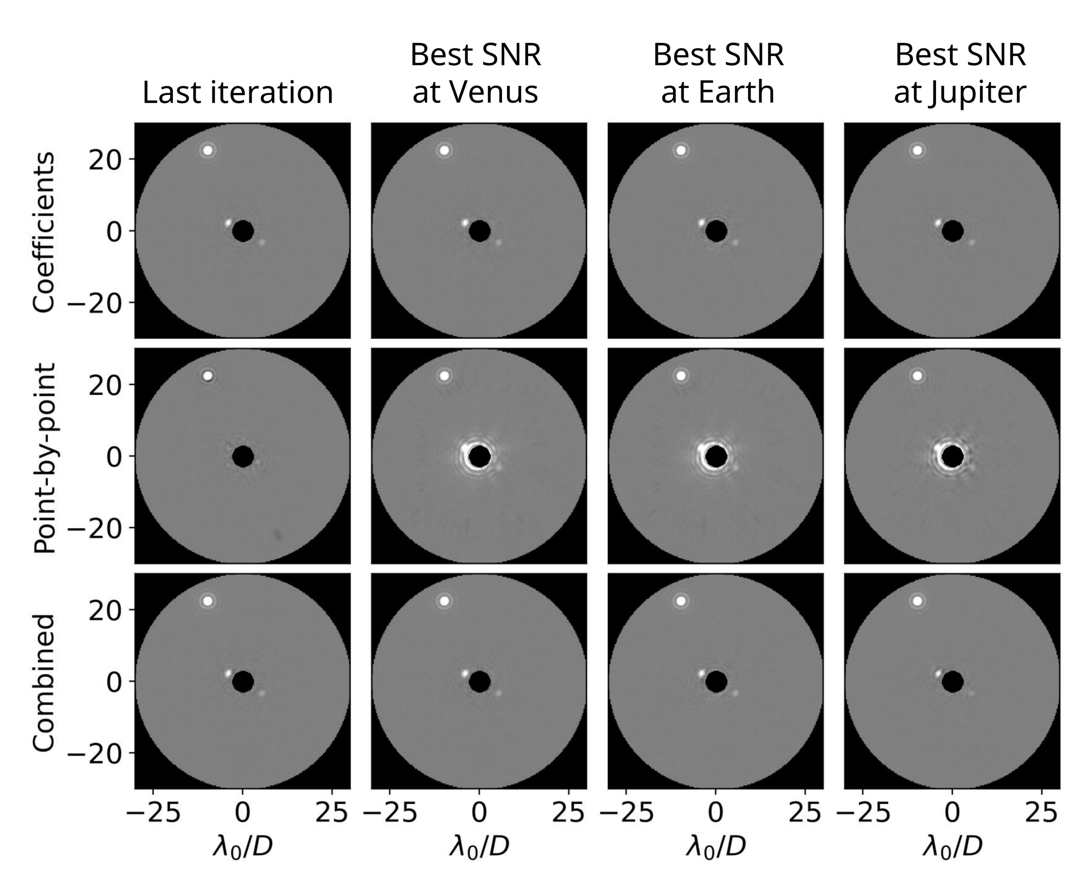

Figure 5. Reduced image for the last iteration and for the iteration with the highest SNR at each planet, for each optimization approach, for Zernike drift of 5pm/10min.

Comparison under wavefront drift

We compared the performance of the GBO approach to two traditional postprocessing approaches: Reference star differential imaging (RDI) [5], and Angular differential imaging (ADI) [6]. We simulated these techniques for cases with different amounts of wavefront drift in both the global Zernike aberrations and the segment alignments.

For the GBO approach, we include the result after 100 iterations of optimizing the aberration coefficients. For RDI we assumed identical point-source stars which were observed for 33.25 hours each. For ADI, we assumed 4 images taken at ±22.5° observed for 16.56 hours each.

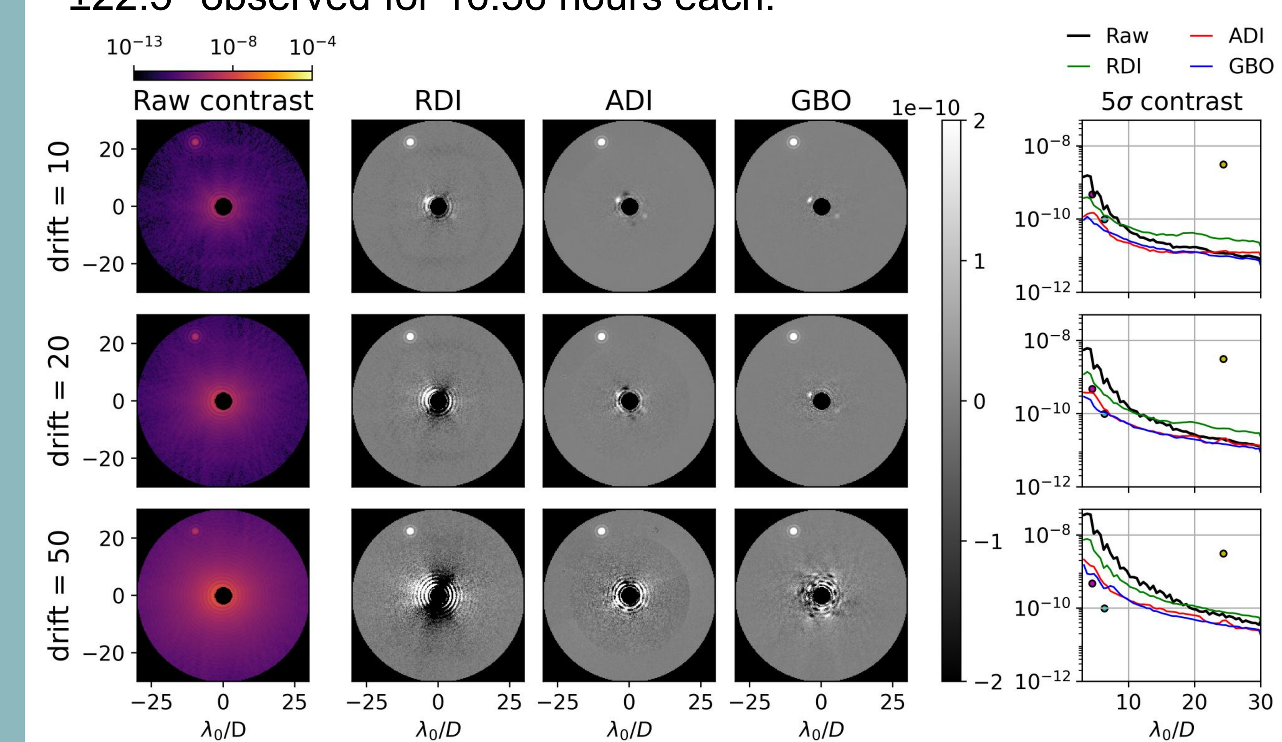

Figure 6. Raw image (left) and final images obtained with each PSF subtraction technique. 5σ contrast curves for the corresponding images (right), for a case with Zernike drift (in units of pm per 10 min), and static segment misalignments.

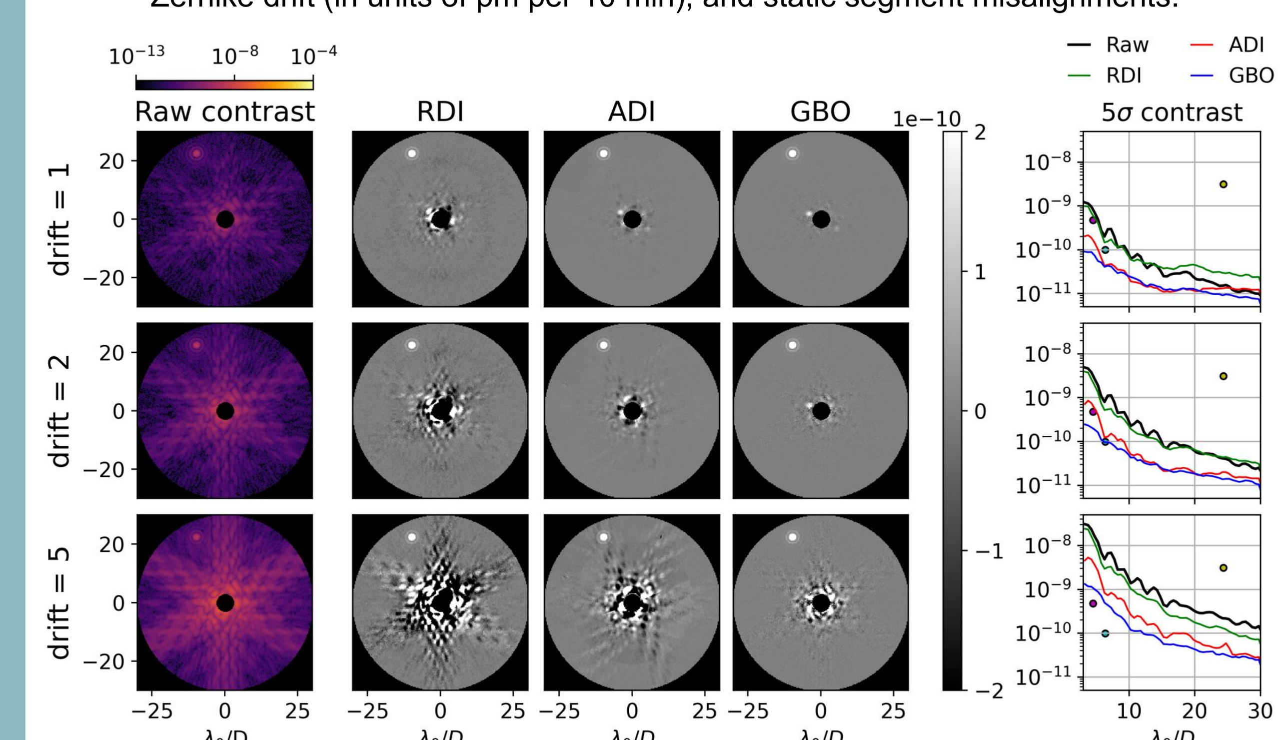

Figure 7. Raw image (left) and final images obtained with each PSF subtraction technique. 5σ contrast curves for the corresponding images (right), for a case with segment alignment drift (in units of pm per 10 min), and static Zernike aberrations.

Conclusion

Our simulations so far show that a gradient-based optimization approach can achieve a performance similar to that of conventional postprocessing methods, but without moving the telescope. Even with a drifting wavefront, using a single wavefront estimate with a GBO approach can achieve a solution that has a similar performance to other techniques.

Further work is required to optimize this method, and to account for other factors that might affect its performance. So far, our coronagraph model matches the model we used to simulate the target image exactly. In future work we will analyze the effect of model mismatch on this approach. We will also study the performance of this approach assuming no previous planet location information. Lastly, only phase aberrations have been included in the model so far. We will study this approach accounting for both amplitude and phase errors.

References and acknowledgments

References

[1] B. Y. Feng et al., "Exoplanet imaging via differentiable rendering," IEEE Trans. Comput. Imaging 11, 36–51 (2025) [doi:10.1109/TCI.2025.3525971].

[2] D. P. Mawet et al., "Apodized vortex coronagraph for the Habitable Worlds Observatory," Proc. SPIE 13627, 136271A-1 (2025) [doi:10.1117/12.3065779].

[3] J. Z. Lou et al., "Habitable World Observatory modeling optical and metrology models, and performance predictions," Proc. SPIE 13129, 131290K (2024) [doi:10.1117/12.3030015].

[4] A. Give'on et al., "Broadband wavefront correction algorithm for high-contrast imaging systems," Proc. SPIE 6691, 66910A [doi:10.1117/12.733122].

[5] D. Lafrenière et al., "HST /NICMOS detection of HR 8799 b in 1998," ApJ 694(2), L148–L152 (2009) [doi:10.1088/0004-637X/694/2/L148].

[6] C. Marois et al., "Angular differential imaging: a powerful high-contrast imaging technique," ApJ 641(1), 556–564 (2006) [doi:10.1086/500401].

Acknowledgments

This research was funded by NASA grant 80NSSC24K1098.
We thank Scott Will for helpful discussions.